Am J Cancer Res 2026;16(8):3377-3393
www.ajcr.us /ISSN:2156-6976/ajcr0171297

*Original Article*

# Treating T24 cells with erianin restores gefitinib drug sensitivity by regulating MYLK to inhibit EGFR and EMT processes

Fubo Li[1], Yan Guo[2], Zhuangyu Xu[1], Wenxin Li[1], Yi Dong[1], Fan Xu[1]

[1]*Department of Oncology, Affiliated Hospital of Chengde Medical University, Chengde 067000, Hebei, China;*
[2]*Department of Oncology, The First People's Hospital of Nanning, Nanning 530000, Guangxi, China*

Received January 7, 2026; Accepted July 27, 2026; Epub August 15, 2026; Published August 30, 2026

**Abstract:** Erianin exerts anticancer effects in bladder cancer, although its underlying molecular mechanisms remain unclear. This study used online databases to identify erianin-related drug targets and bladder cancer-associated disease targets and to predict the potential signaling pathways involved. Intersecting genes were enriched in the epidermal growth factor receptor (EGFR) tyrosine kinase inhibitor resistance signaling pathway, and high myosin light chain kinase (MYLK) expression was associated with poor prognosis. A gefitinib-resistant bladder cancer cell line was established to evaluate the role of MYLK. Erianin inhibited MYLK and EGFR protein expression, blocked EGFR signaling and epithelial-mesenchymal transition (EMT), restored gefitinib sensitivity, and suppressed the proliferation, invasion, and migration of bladder cancer cells.

**Keywords:** Erianin, T24, myosin light chain kinase, epidermal growth factor receptor, epithelial-mesenchymal transition

## Introduction

Urothelial carcinoma (UC) is a common malignant tumor of the urinary system [1]. Transitional cell carcinoma (TCC) accounts for approximately 95% of bladder cancer cases [2]. Current treatment options for bladder cancer include surgery, chemotherapy (gemcitabine + cisplatin), immunotherapy (durvalumab, and pembrolizumab), and targeted therapy (erdafitinib, and enfortumab vedotin) [3-6]. Epithelial-mesenchymal transition (EMT), which often occurs during invasion and metastasis in epithelial tumors, confers a mesenchymal phenotype and contributes to drug resistance in bladder cancer. Through EMT, tumor cells can enhance self-repair capacity and resist chemotherapy-induced damage [7-9], leading to treatment failure and reduced survival. However, current treatment methods remain limited. Phenformin combined with gefitinib inhibits bladder cancer progression by suppressing EGFR and AMPK pathways. Gefitinib can reverse abnormal EGFR pathway activation and PD-L1-mediated immunosuppression induced by long-term glutamine blockade in bladder cancer. These indicate that gefitinib, an EGFR inhibitor, suppresses the proliferation, invasion, and migration of bladder cancer cells and has research value in the study of bladder cancer. The widespread expression of EGFR in bladder cancer, together with gefitinib's capacity to reverse drug resistance and support combination therapy, makes gefitinib a promising candidate for addressing the limitations of conventional treatment [10-12].

Inhibiting EMT-related genes can reverse the invasive and metastatic capacity of bladder cancer cells [13, 14]. Therefore, drugs targeting EMT-related genes may provide an effective strategy for bladder cancer treatment. Combining chemotherapeutic agents with EMT-targeted drugs may improve chemotherapy efficacy and reduce drug resistance [15, 16]. Therefore, EMT has become an important focus of anticancer research. Natural compounds are important sources for developing low-toxicity and highly effective anticancer drugs. Erianin, a plant-derived compound, has antitumor [17],

https://doi.org/10.62347/YZXW4438

antioxidant [18], and anti-inflammatory properties [19]. Erianin significantly inhibits cancer cell growth and proliferation, and its mechanism is associated with inhibition of EMT. Erianin downregulates N-cadherin expression and upregulates E-cadherin expression, thereby inhibiting EMT [20]. Erianin also inhibits the PI3K/AKT signaling pathway, thus preventing hepatocellular carcinoma metastasis and invasion [21]. However, its mechanism of action in bladder cancer remains unclear.

The present study used bioinformatics analysis to predict the targets and signaling pathways of erianin in bladder cancer, focusing on the myosin light chain kinase (MYLK) and the epidermal growth factor receptor (EGFR) resistance signaling pathway. High MYLK expression has been associated with poor prognosis in several cancer types and can induce EMT in cancer cells [22, 23]. Gefitinib is an epidermal growth factor receptor tyrosine kinase inhibitor (EGFR-TKI), and resistance to gefitinib occurs in several cancers [24]. Identifying targets involved in gefitinib resistance is therefore essential. This study investigated the effect of erianin on EMT in T24/gefitinib-resistant (GR) bladder cancer cells and explored its preliminary mechanism of action.

## Methods and materials

### *Screening and pathway enrichment analysis of erianin and bladder cancer targets*

A total of 116 erianin-related drug targets were obtained from the CTD database (https://ctdbase.org/) by searching for "erianin" and using Swiss Target Prediction (http://swisstargetprediction.ch/) (Table S1). Bladder cancer-related genes were retrieved from the GeneCards database (https://www.genecards.org/) using "bladder cancer" as the keyword, yielding 11,828 targets. Targets with relevance scores greater than or equal to the median score (7.81) were retained, resulting in 3,383 bladder cancer-related target genes (Table S2) [25, 26]. The VennDiagram package in R was utilized to identify overlapping genes between the two datasets and generate a Venn diagram, yielding 63 intersecting genes. The DAVID Bioinformatics Resources online database (https://david.ncifcrf.gov/summary.jsp) was used to perform Kyoto Encyclopedia of Genes and Genomes (KEGG) and Gene Ontology (GO) enrichment analyses of the 63 intersecting genes [27].

### *Screening of potential target genes for erianin and bladder cancer*

The GSE13507 dataset (primary bladder cancer and adjacent carcinoma) was downloaded from NCBI (https://www.ncbi.nlm.nih.gov/) and analyzed using the R packages "FactoMineR" and "factoextra". Principal component analysis was performed on the two sample groups, and differential expression between groups was analyzed using the "limma" package. Genes were screened using $P < 0.05$ and $|logFC| > 1$, yielding 385 differentially expressed genes, including 52 upregulated and 333 downregulated genes (Table S3) [28]. The two groups formed distinct clusters, and differentially expressed genes were used to generate volcano plots and clustering heat maps [29].

For molecular docking, core ligand structure files were retrieved in SDF format from PubChem (CID: 356759; https://pubchem.ncbi.nlm.nih.gov). The MYLK protein structure was selected using the following criteria: resolution standard ≤ 2.5 Å to ensure clear electron density for binding-pocket residues and reduce conformational ambiguity; no more than three consecutive missing key residues; active ligand threshold ≤ -5.0 kcal/mol; conformational similarity threshold RMSD ≤ 2.0 Å; and minimum cluster proportion ≥ 60%. These criteria were used to exclude random binding patterns and ensure reproducibility. The ligand files were converted into PDB files using PyMOL 2.5.8 (https://pymol.org/2/). The 3D crystal structures of the targets were obtained from the RCSB Protein Data Bank (https://www.pdb.org/) and imported into PyMOL 2.5.8 for water molecule removal and ligand separation [30]. Ligands and receptors were imported into AutoDock Tools 1.5.6 (https://ccsb.scripps.edu/mgltools/downloads/) for dehydration, hydrogenation, and charge calculation and were saved in pdbqt format. Molecular docking was performed using AutoDockVina to obtain binding energy data for each active ingredient-target pair, and components and targets with favorable binding activities were selected based on binding energy [31]. Finally, PyMol version 2.5.8, and Discovery Studio 2019 were used to visualize the docking results.

Using the genes obtained from GeneCards and Swiss Target Prediction, intersecting genes were visualized with a Venn diagram generated

using the VennDiagram package in R. Online analysis software (https://www.xiantaozi.com/literatures) was used to generate prognostic survival curves for bladder cancer [32].

*Cell culture*

Human invasive uroepithelial cancer cells (T24 cells) were purchased from the Shanghai Cell Bank of the Chinese Academy of Sciences. After removal from liquid nitrogen, T24 cells were resuspended, cultured in McCoy's 5A medium containing 10% fetal bovine serum (FBS) and 1% penicillin-streptomycin, and passaged every 2 days. Cells were cultured until the exponential growth phase before subsequent experiments. Gefitinib (HY-50895) and erianin (HY-N0517) were purchased from MedChem Express Biotechnology Inc. (Monmouth Junction, NJ, USA). Before the experiments, the cell lines were authenticated by an expert and confirmed to be free of mycoplasma contamination.

*Construction of T24/GR cell line*

Cells in logarithmic growth phase (80%-90% confluence) were treated with gefitinib at an initial concentration of 1/10-1/5 of the $IC_{50}$ of the parental cell line and cultured at 37°C with 5% $CO_2$. When cell density reached 50%, the medium was replaced with drug-free medium for continued incubation. When cell density returned to 80%-90%, the drug treatment was repeated 6-8 times. The drug concentration was increased after stable cell growth, and the same procedure was repeated until cells grew stably at the final drug concentration. The $IC_{50}$ of the drug-resistant cell line was calculated. A resistance index (RI) > 5 (RI = $IC_{50}$ of resistant cell line/$IC_{50}$ of parental cell line) indicated successful establishment of a resistant strain. T24 cells represented the parental cell line, and T24/GR cells represented the GR strain. After successful construction, T24/GR cells were cultured in McCoy's 5A medium containing 100 nmol/L gefitinib to maintain drug resistance.

*Construction of MYLK overexpression and downregulation cell lines*

To construct the MYLK over-expression plasmid, pcDNA3.1(+) vector was linearized by double digestion with BamHI and EcoR I. In-Fusion® HD cloning (639649; Clontech, China) was performed using primers with homologous arms to amplify the full-length CDS of MYLK gene. After gel recovery, the amplified product and linearized vector were homologously recombined. The recombinant product was transformed into TOP10 competent cells (CB104-01; TIANGEN BIOTECH (BEIJING) Co., Ltd., China), plated on resistant LB plates, and cultured, after which single colonies were selected. Positive clones were verified by colony PCR and sequencing, and recombinant plasmids were extracted. Specific siRNAs targeting MYLK were designed by General Biosystems (Anhui) Corp. Ltd. T24/GR cells in exponential phase were collected, centrifuged, resuspended, and seeded into six-well plates at $3 \times 10^5$ cells/mL; 2 mL of cell suspension was added to each well and incubated overnight. The following day, siRNA or overexpression plasmid mixed with Lip3000 transfection reagent (Thermo Fisher Scientific, L3000075, China) was added. Cells were collected 48 h after transfection for subsequent experiments, and successful construction was confirmed by quantitative polymerase chain reaction (qPCR) and western blotting.

*Cell counting kit-8 assay*

When T24 cells reached exponential phase, 1 mL of trypsin (P6730; Solarbio, China) was added, and cells were incubated for 2-3 min. McCoy's 5A medium (1 mL; Solarbio, M9420) was then added, and the mixture was centrifuged at 1200 rpm for 3 min. Subsequently, 3,000 cells were seeded into 96-well plates and incubated overnight. Experimental groups were treated with different concentrations of erianin or gefitinib, and the control group received the same volume of dimethyl sulfoxide. After 48 h of incubation in an incubator (Thermo Fisher Scientific, Heracell Vios 160i CR), 10 μL of Cell Counting Kit-8 (CCK8; Solarbio, CA1210) solution was added to each well. After a further 3 h of incubation, absorbance at 450 nm was measured using a microplate reader (Flash, ReadMax 1200).

*Wound healing assay*

Successfully transfected T24/GR cells were collected, digested, and counted at a concentration of $5 \times 10^5$ cells/mL per well, then inoculated into six-well plates. Then, 1 mL of cell suspension was added to each well, and 1 mL of McCoy's 5A medium was replenished. The cells

were then incubated overnight. Three lines were drawn horizontally using a pipette gun with a 10 μL tip, and the dislodged cells were washed away with phosphate-buffered saline (PBS). The cells were then added to a cell culture incubator containing 100 nmol/L erianin. McCoy's 5A medium was added, and the cells were re-incubated, after which they were photographed using a microscope, placed in a cell culture incubator, and incubated for 24 h. The cells were then removed and photographed under a microscope (Thermo Fisher Scientific, EVOS™ M7000), and the healing rate was calculated using statistical analysis using ImageJ 1.5.2a software.

*Transwell assay*

Matrigel (356234; BD Biosciences, China) was diluted with serum-free McCoy's 5A medium at a ratio of 1:11. A 100-μL aliquot of the diluted matrix was added to the upper Transwell chamber, and 500 μL of McCoy's 5A medium containing 20% FBS was added to the lower chamber. Successfully transfected T24 cells were collected and diluted to $1 \times 10^5$ cells/mL. A 50-μL cell suspension was added to the upper chamber, followed by 50 μL of serum-free McCoy's 5A medium containing 200 nM erianin. After 12 h of culture, cells were fixed with 500 μL of methanol in each lower chamber for 25 min. Excess methanol was removed by washing with PBS. A 0.1% crystal violet solution (Solarbio, G1062) was added to each lower chamber and incubated for 25 min. Excess crystal violet was removed by washing with PBS, and three randomly selected fields were photographed under a microscope.

*Immunofluorescence assay*

Transfected T24/RG cells were seeded onto cell coverslips. After attachment, the cells were incubated with 100 nM erianin for 48 h, fixed with 4% paraformaldehyde, and washed three times with PBS. Triton X-100 (0.5%; Solarbio, T8200) was then added, and cells were incubated at 25°C for 20 min. Bovine serum albumin (Solarbio, T8010) was added and incubated at room temperature for 1 h, followed by incubation with the corresponding primary antibodies. The cells were washed three times with PBS, incubated with fluorescent secondary antibody in a wet box protected from light for 1 h, washed three times with PBS, stained with 4',6-diamidino-2-phenylindole, and incubated protected from light for 5 min. After three additional PBS washes, mounting medium was added. After air drying, cells were photographed using a confocal microscope (Leica, STELLARIS 5 Cryo), and three randomly selected images were quantitatively analyzed using ImageJ 9.0. Details of antibody and dilution ratios are presented in Table S4.

*qPCR assay*

Cell precipitates were collected according to the requirements of each group, and total RNA was extracted using TRIzol reagent (Solarbio, R1200) according to the manufacturer's instructions. Complementary DNA was synthesized using Hifair II 1st Strand cDNA Synthesis SuperMix (Yeasen, Shanghai, China). qPCR was performed on a LightCycler 480 Instrument II (Roche) using Hieff® qPCR SYBR Green Master Mix (Yeasen). Data were analyzed using GraphPad Prism 10.0.1. The qPCR primer sequences, si-MYLK interference sequences, and overexpression sequence information are listed in Table S5.

*Western blot assay*

Cell precipitates were collected, and tissue cell lysate (Solarbio, BC3710) was added. Protein concentration was determined using a BCA kit (Solarbio, PC0020) according to the manufacturer's instructions. Extracted proteins were heated at 95°C for 15 min, cooled to room temperature, and used immediately or stored at -80°C. Protein samples were loaded into each well, separated by gel electrophoresis at 120 V for 90 min, and transferred onto polyvinylidene fluoride membranes at 220 V for 30 min. The membranes were blocked with 5% skim milk powder for 2 h, incubated with primary antibodies overnight, washed with Tris-buffered saline with Tween 20 (TBST), and incubated with secondary antibody for 1 h. After washing again with TBST, the membranes were placed in chemiluminescent solution for 10 s and imaged using an iBright FL1500 Imaging System (Thermo Fisher Scientific, A44241). Details of the antibody and dilution ratios are provided in Table S4.

*Co-immunoprecipitation assay*

Cell pellets were collected, and tissue cell lysis buffer was added to obtain total protein extracts. The supernatant was incubated over-

night with a specific antibody at 4°C. Protein A/G agarose beads were added, and incubation was continued at 4°C for 2 h to bind the antibody-antigen complex (Beyotime Biotech Inc., P2197M, China). The agarose beads were thoroughly washed with buffer and eluted. The eluate was collected, and the immunoprecipitated protein complex was analyzed by sodium dodecyl sulfate-polyacrylamide gel electrophoresis and western blotting to verify protein interactions.

*Cell derived xenograft*

Male nude mice (6-7 weeks old, weighing 20-24 g) were purchased from Henan Skebes Biotechnology Co., Ltd. (Henan, China). All animal procedures were approved by the Institutional Animal Care and Use Committee of Chengde Medical University (approval No. CYFYLL2025704). Tumor cell suspensions were prepared in 100 μL of PBS, and each mouse was subcutaneously injected with 5 × $10^6$ tumor cells into the dorsal flank. Subsequently, the mice were randomly divided into four groups (n = 6 per group). Tumor growth was monitored every three days by measuring the long and short axes of the tumors using a caliper, and tumor volume was calculated using the formula: volume = (major axis × minor axis$^2$)/2. When the tumor volume reached approximately 100 mm$^3$, the four groups-Control, Erianin, Gefitinib, and Erianin + Gefitinib-were administered normal saline, erianin (100 mg/kg, intraperitoneal injection), gefitinib (50 mg/kg, oral gavage), and the combination of erianin and gefitinib, respectively. At the end of the experiment, all mice were euthanized by cervical dislocation under deep anesthesia induced by intraperitoneal injection of pentobarbital sodium (50 mg/kg). Death was confirmed by cessation of breathing and heartbeat, as well as loss of pedal withdrawal reflex.

*Statistical analysis*

Statistical analyses were conducted using SPSS software (version 20.0, IBM Corp., Armonk, NY, USA). All data are presented as the mean ± standard deviation (SD) from at least three independent experiments. For comparisons between two groups, the two-tailed unpaired Student's *t*-test was employed. For comparisons involving more than two groups, one-way analysis of variance (ANOVA) followed by Tukey's post hoc test was used for multiple comparisons. The dose-response curves for $IC_{50}$ calculations were fitted using nonlinear regression analysis. Survival curves were generated using the Kaplan-Meier method, and differences between groups were assessed by the log-rank test. A *P*-value < 0.05 was considered statistically significant, with significance levels denoted as $P < 0.05$, $P < 0.01$, $P < 0.001$, and $P < 0.0001$; "ns" indicates not significant ($P > 0.05$).

## Results

*Prediction of potential signaling pathways for erianin*

Relevant data were downloaded from online databases to identify potential therapeutic targets of erianin in bladder TCC and determine the overlap between predicted erianin targets and bladder cancer-related targets. A total of 63 overlapping genes were identified (**Figure 1A**). GO enrichment analysis showed that PI3K-related enzyme activities and complexes were primarily enriched (**Figure 1B**). Conversely, KEGG functional enrichment analysis revealed that the differentially expressed genes were primarily enriched in non-small cell lung cancer, EGFR tyrosine kinase inhibitor resistance, gliomas, and endocrine resistance pathways (**Figure 1C**).

*Prediction of potential erianin targets*

The principal components of the GSE13507 dataset were analyzed (**Figure 2A**), and volcano plots (**Figure 2B**) and cluster heatmaps (**Figure 2C**) were generated. No additional relevant information was obtained. GSE13507 target information was collected and intersected with erianin and disease targets. The Venn diagram identified two intersecting genes: MYLK and aurora kinase A (AURKA) (**Figure 2D**). Prognostic survival analysis in bladder cancer revealed that patients with high MYLK expression had worse prognosis than patients with low MYLK expression ($P < 0.001$), whereas survival did not differ significantly between patients with high and low AURKA expression (**Figure 2E** and **2F**). Analysis based on the TCGA database revealed that MYLK gene expression is significantly upregulated in tumor tissues, and its expression levels show a stepwise increase with the progression of bladder cancer clinical

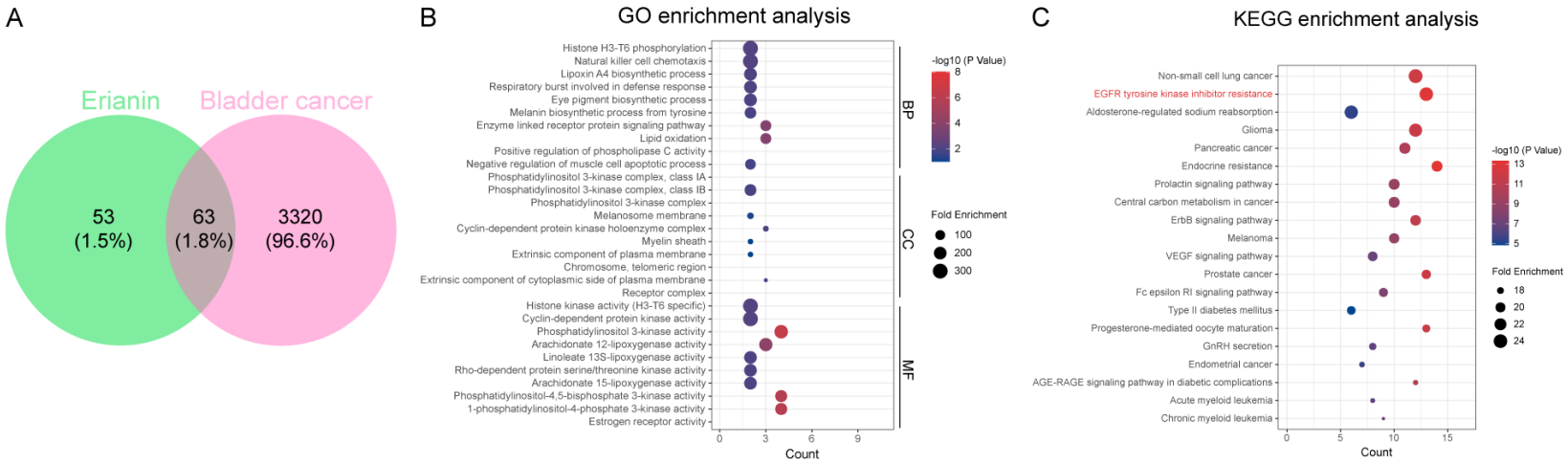


**Figure 1.** Analysis of the predictive targets of erianin and bladder cancer. The intersecting predicted genes of erianin and bladder cancer targets were used to (A) draw the Venn diagram, as well as (B) perform Gene Ontology, and (C) Kyoto Encyclopedia of Genes and Genomes functional enrichment analyses.

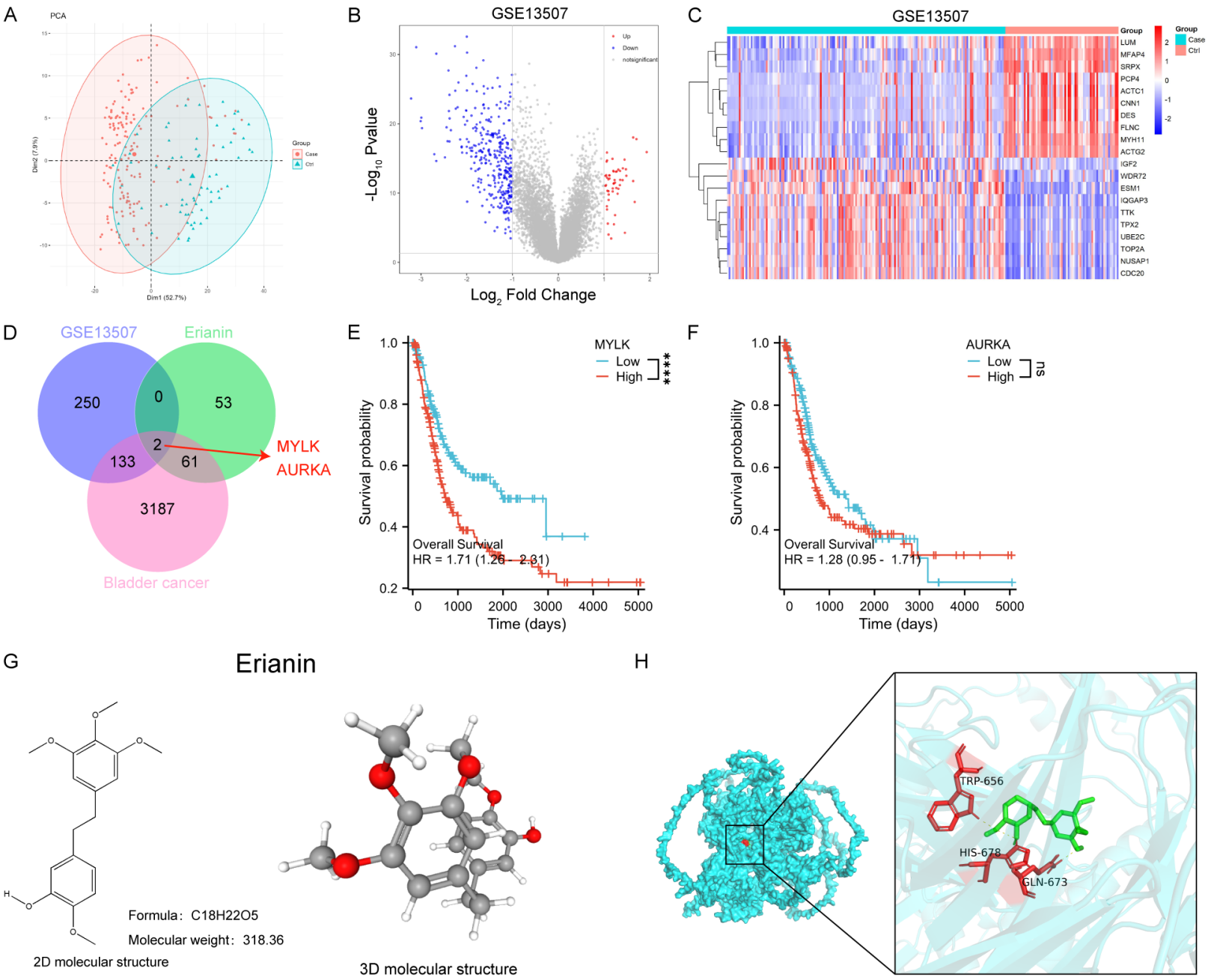
A
PCA
Group
Case
Ctrl
Dim1 (52.7%)
Dim2 (7.9%)
B
GSE13507
Up
Down
notsignificant
-Log10 Pvalue
Log2 Fold Change
C
GSE13507
Group
Case
Ctrl
LUM
MFAP4
SRPX
PCP4
ACTC1
CNN1
DES
FLNC
MYH11
ACTG2
IGF2
WDR72
ESM1
IQGAP3
TTK
TPX2
UBE2C
TOP2A
NUSAP1
CDC20
D
GSE13507
Erianin
Bladder cancer
250
0
53
2
133
61
3187
MYLK
AURKA
E
MYLK
Low
High
****
Survival probability
Overall Survival
HR = 1.71 (1.26 - 2.31)
Time (days)
F
AURKA
Low
High
ns
Survival probability
Overall Survival
HR = 1.28 (0.95 - 1.71)
Time (days)
G
Erianin
Formula: C18H22O5
Molecular weight: 318.36
2D molecular structure
3D molecular structure
H
TRP-656
HIS-678
GLN-673

**Figure 2.** Predictive target screening of erianin for the treatment of bladder cancer. A. Principal component analysis plot of the GSE13507 disease database. B. Volcano plot of differentially expressed genes in the GSE13507 disease database. C. Clustering heatmap of the top 10 upregulated and downregulated genes in the GSE13507 disease database. D. Venn diagrams of the intersection of the target genes obtained from the three online databases. E. Prognostic survival analysis of myosin light chain kinase (MYLK) expression in patients with bladder cancer. F. Prognostic survival analysis of aurora kinase A (AURKA) expression in patients with bladder cancer. G. 2D and 3D molecular structure of erianin and its relative molecular mass. H. Schematic diagram of molecular docking of erianin and MYLK proteins. When comparing the two groups, $****P < 0.0001$ indicates significance, whereas "ns" with $P > 0.05$ represents no significance.

stages (from stage II to stage IV). This confirms that MYLK is not only a driver of tumorigenesis but also a critical biomarker of disease progression (Figure S1). Therefore, the MYLK factor, which has prognostic significance, was selected as the primary subject of subsequent analyses. The 2D and 3D molecular formulae of erianin are shown in **Figure 2G**. The molecular docking of erianin with MYLK revealed a corresponding binding site between the two. The docking binding energy between erianin and the MYLK protein was -5.72 kcal/mol. Erianin formed a hydrogen bond with the amino acid residue GLN673 on the protein and formed hydrophobic interactions with the amino acid residues HIS678 and TRP656 (**Figure 2H**).

*Erianin inhibits T24/GR cell viability*

The effect of erianin on cell viability was investigated in bladder cancer and normal cell lines to determine whether erianin could restore gefitinib sensitivity. Erianin inhibited the proliferation of multiple bladder cancer cell lines, with the strongest inhibitory effect observed in T24 cells. In contrast, erianin had no significant inhibitory effect on the normal SV-HUC-1 cell line, indicating selective cytotoxicity toward bladder cancer cells (Figure S2).

To further verify whether erianin restored gefitinib sensitivity, T24 cells were selected because the $IC_{50}$ of erianin in these cells (147.28 nmol/L) was lower than that in the other bladder cancer cell lines. T24/GR cells were then established. The $IC_{50}$ values of gefitinib in T24 and T24/GR cells were 0.1534 μmol/L and 1.703 μmol/L, respectively, and RI = 11.1 > 5 indicated successful construction of the T24/GR cell line (**Figure 3A**). In addition, erianin inhibited T24/GR cell viability in a concentration-dependent manner, with an $IC_{50}$ of 106.29 nmol/L (**Figure 3B**). To evaluate erianin activity within the effective concentration range and avoid potential cytotoxicity, 100 nmol/L was selected for subsequent experiments based on the $IC_{50}$ in T24/GR cells [33, 34]. Western blotting confirmed higher MYLK, EGFR, and p-EGFR expression in T24/GR cells than in T24 cells (**Figure 3C**). T24/GR cell lines with upregulated or downregulated MYLK expression were constructed to confirm the regulatory roles of erianin and MYLK (**Figure 3D** and **3E**). CCK8 results showed that MYLK overexpression enhanced T24/GR cell viability and weakened the inhibitory effect of erianin. After MYLK downregulation, T24/GR cell viability was significantly reduced (**Figure 3F**).

*Erianin inhibits EMT in T24/GR cells*

The effects of erianin on invasion, migration, and EMT in T24/GR cells were investigated. Scratch and Transwell assays showed that migration and invasion were significantly decreased in the erianin group compared with the control group. Cell migration and invasion ability were also significantly increased in the MYLK overexpression group compared with that in the control group, and MYLK overexpression attenuated the inhibitory effect of erianin on T24/GR cell invasion. The si-MYLK group exhibited significantly decreased invasion and migration compared with the control group. Erianin treatment for 24 h after successful si-MYLK transfection did not significantly alter cell migration or invasion compared with erianin treatment alone (**Figure 4A** and **4B**). E-cadherin and N-cadherin expression was then assessed by immunofluorescence (**Figure 5A** and **5B**) and western blotting (**Figure 6A** and **6B**). E-cadherin and N-cadherin were expressed in both the cytoplasm and nucleus, and erianin upregulated E-cadherin and downregulated N-cadherin by inhibiting MYLK expression.

*Erianin inhibits EGFR signaling and EMT through downregulation of MYLK*

After confirming that erianin can inhibit the proliferation, invasion, migration, and EMT process of T24/GR cells, further investigation focused

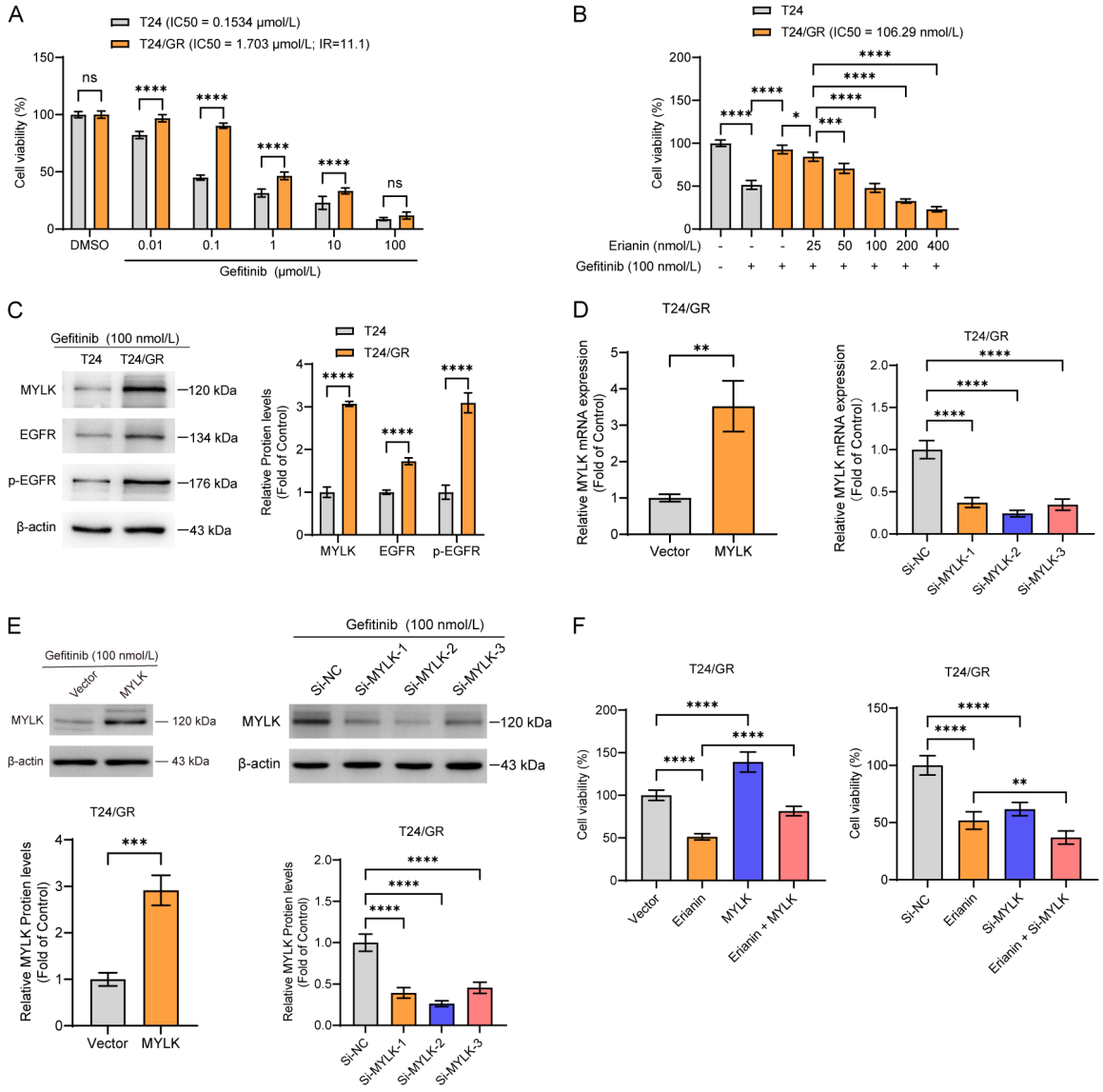


**Figure 3.** Erianin inhibits T24/GR cell viability by regulating MYLK protein expression. A. Cell Counting Kit-8 (CCK8) assay to detect the changes in cell viability after T24 and T24/GR cells were treated with different concentrations of gefitinib for 48 h. B. CCK8 assay to detect the changes in cell viability after T24/GR cells were treated with different concentrations of erianin for 48 h. C. Western blot assay to detect the changes in cell viability after treating T24 and T24/GR cells with gefitinib (100 nmol/L) for 48 h to detect MYLK, EGFR, and p-EGFR protein expression. D. Quantitative polymerase chain reaction (qPCR) assay to detect the MYLK mRNA expression level after transfecting T24/GR cells with MYLK overexpression plasmids and siRNA for 48 h. E. Western blotting to detect the MYLK protein expression level. F. CCK8 assay to detect changes in cell viability. When comparing the two groups, $*P < 0.05$, $**P < 0.01$, $***P < 0.001$, and $****P < 0.0001$ indicate significance, while "ns" with $P > 0.05$ represents no significance.

on its potential targets and underlying mechanisms of action. Compared to those in the control group, the MYLK, EGFR, and p-EGFR protein expression levels were significantly decreased in T24/GR cells after 48 h of treatment with erianin, and MYLK overexpression counteracted erianin-induced EGFR and p-EGFR protein downregulation. The si-MYLK group also exhibited downregulated EGFR and p-EGFR protein expression compared with that of the control group. Transfection of si-MYLK in T24/GR cells for 48 h, followed by the addition of erianin for 48 h, showed that the inhibitory effect of EGFR and p-EGFR was not significantly downregulated compared to the erianin-treated group (**Figure 6A** and **6B**). The results of co-

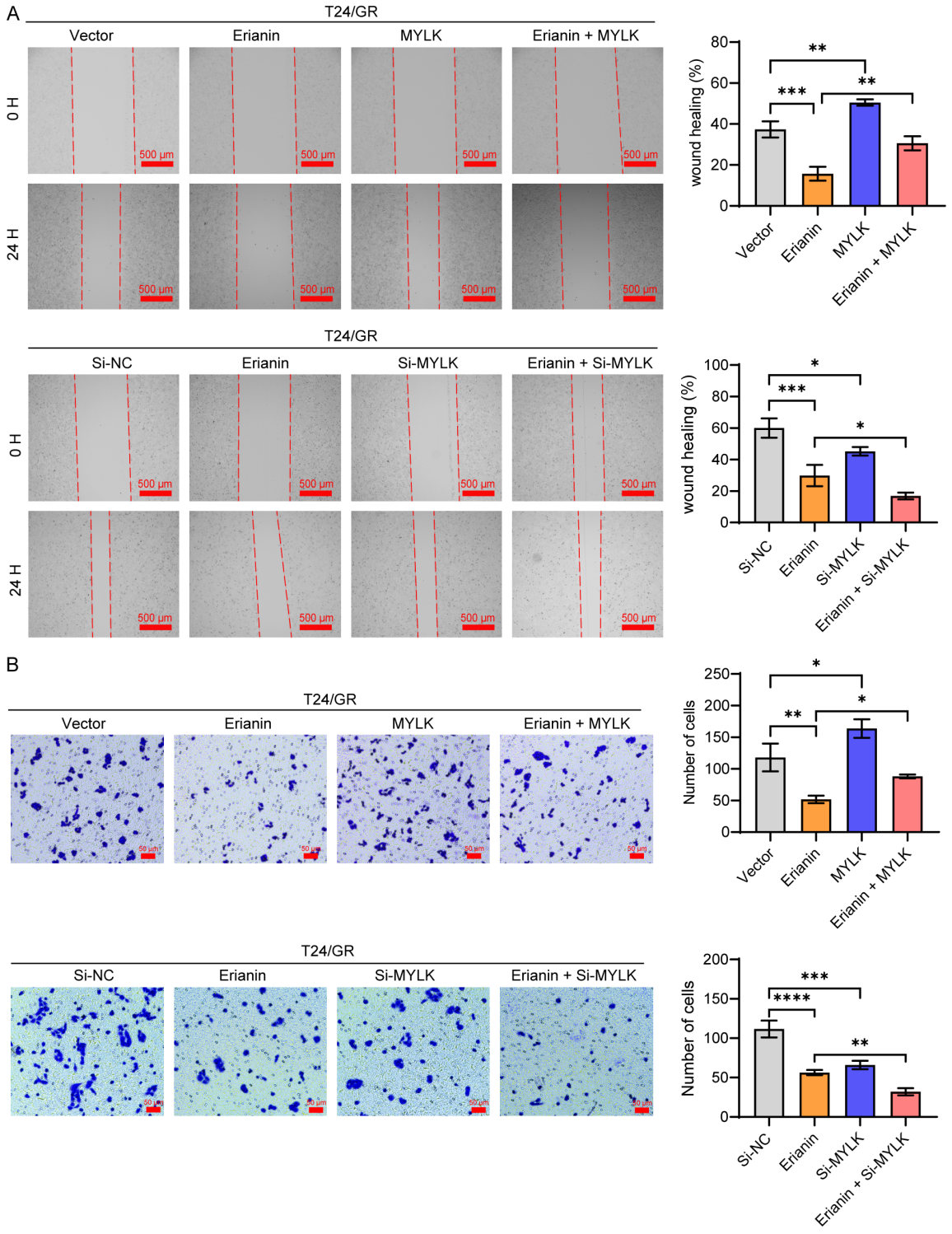


**Figure 4.** Erianin inhibits T24/GR cell invasion and migration by regulating MYLK protein expression. A. Changes in cell migration ability were detected via cell scratch assay 48 h after transfection of T24/GR cells with MYLK overexpression plasmid and siRNA (magnification 4 × 10, scale bar: 500 μm). B. Changes in cell invasion ability detected using a Transwell assay (magnification 20 × 10, scale bar: 50 μm). When comparing the two groups, $^{*}P < 0.05$, $^{**}P < 0.01$, $^{***}P < 0.001$, and $^{****}P < 0.0001$ indicate significance.

immunoprecipitation showed that EGFR was present in the protein complex of MYLK, confirming the interaction between the two (Figure S3).

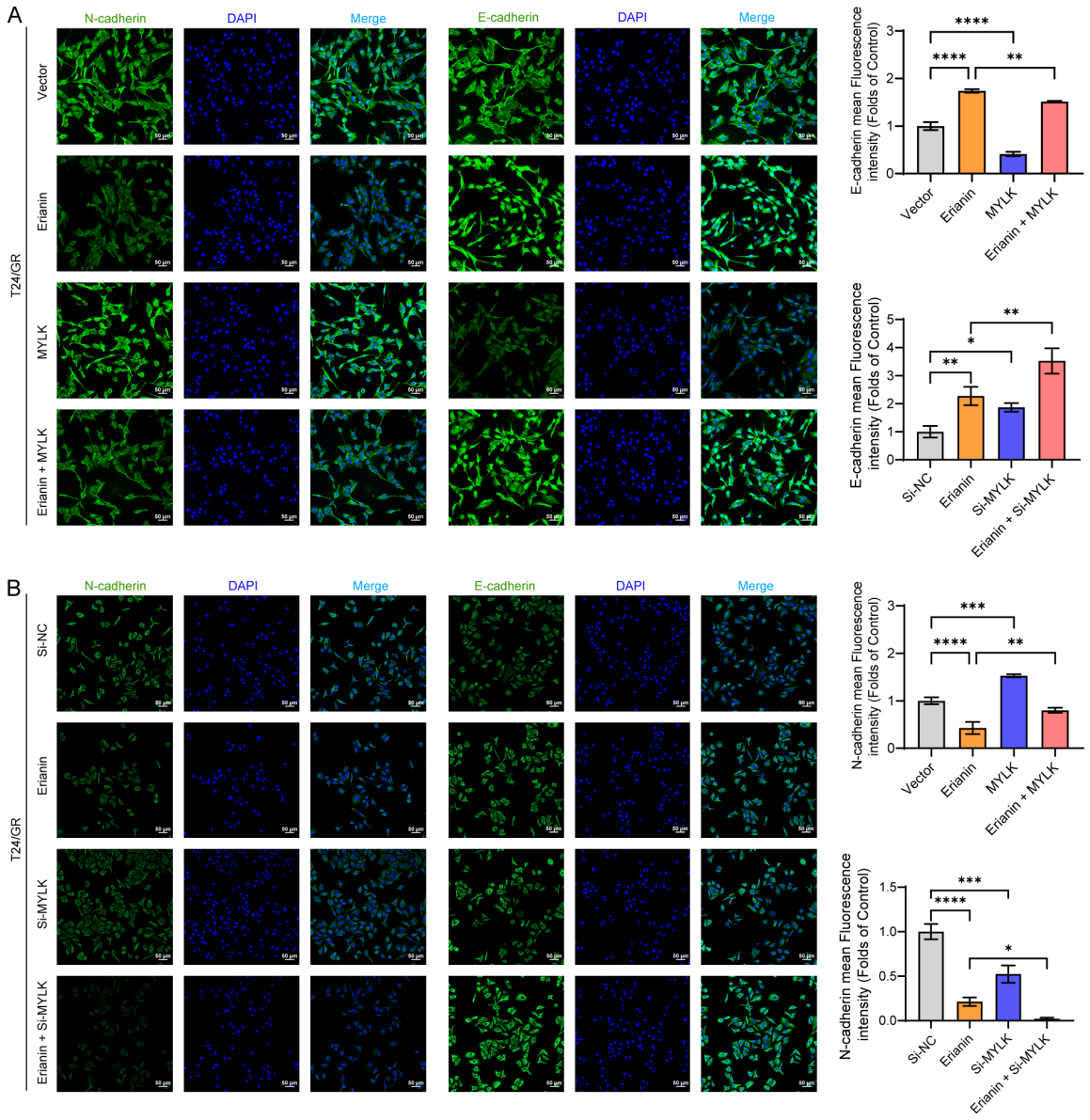


**Figure 5.** Erianin upregulates E-cadherin and downregulates N-cadherin expression levels by regulating MYLK protein expression. A. E- and N-cadherin protein expression using an immunofluorescence assay after transfecting T24/GR cells with a MYLK overexpression plasmid (magnification 20 × 10, scale bar: 50 μm). B. E- and N-cadherin protein expression detected by immunofluorescence assay after transfecting T24/GR cells with MYLK siRNA for 48 h (magnification 20 × 10, scale bar: 50 μm). When comparing the two groups, *$P < 0.05$, ***$P < 0.001$, and ****$P < 0.0001$ indicate significance.

To further verify the functional relationship between MYLK and EGFR in T24/GR cells, we employed erlotinib, a specific EGFR tyrosine kinase inhibitor, as a positive control. As shown in **Figure 6C**, erlotinib treatment alone significantly downregulated EGFR and p-EGFR protein expression levels compared to the vector control group. Notably, MYLK overexpression alone markedly increased the expression of MYLK, EGFR, p-EGFR, and N-Cadherin, while decreasing E-Cadherin expression. However, when MYLK overexpression was combined with erlotinib treatment, the upregulation of EGFR and p-EGFR induced by MYLK overexpression was substantially attenuated, although the inhibitory effect was slightly less potent than that of erlotinib alone. Similarly, the erlotinib-induced downregulation of N-Cadherin and upregulation

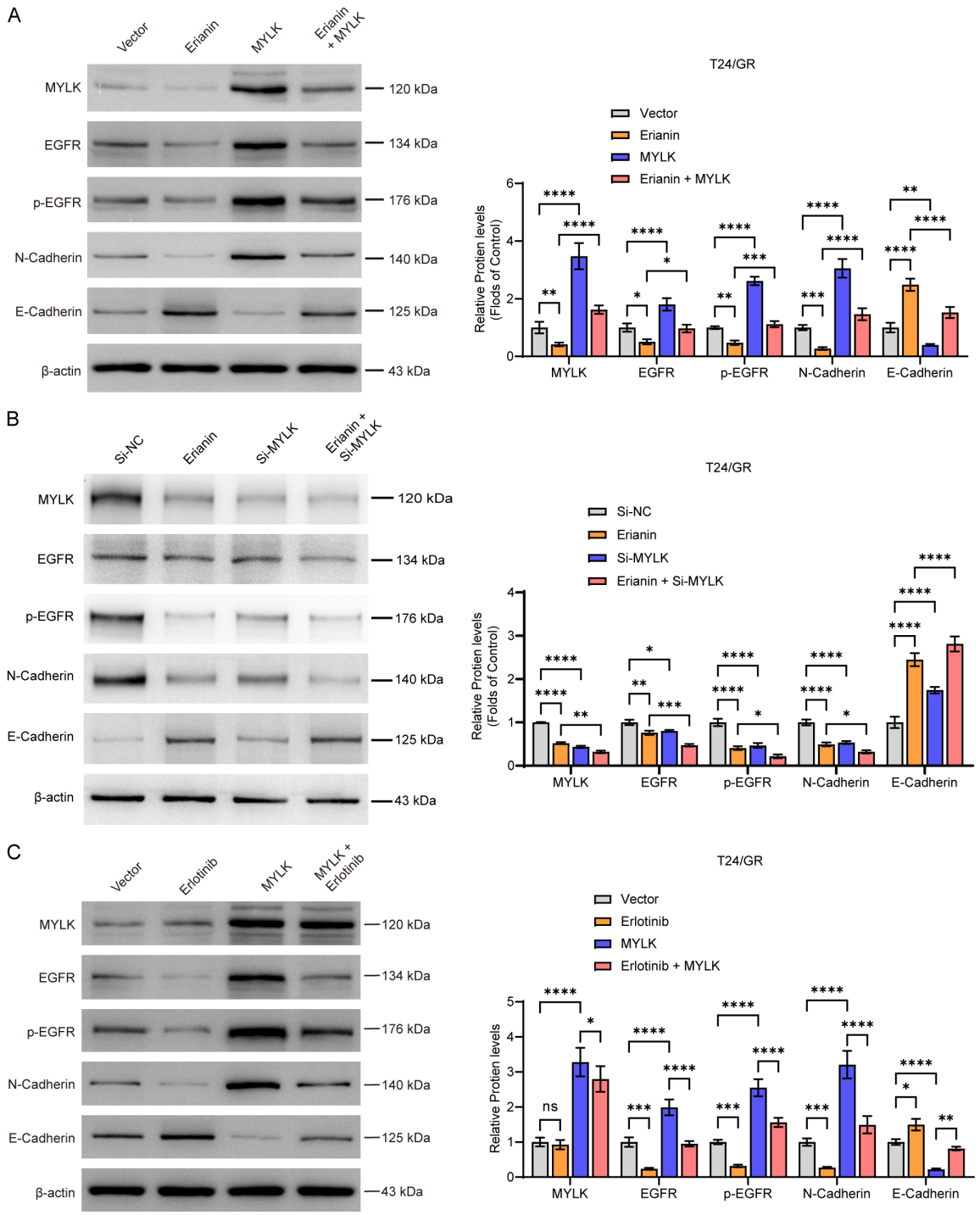


**Figure 6.** Erianin regulates epidermal growth factor receptor (EGFR) and epithelial-mesenchymal transition-related protein expression. A. Western blot assay used to detect MYLK, EGFR, p-EGFR, E-cadherin, and N-cadherin protein expression after transfecting T24/GR cells with a MYLK overexpression plasmid. B. Western blot assay to detect MYLK, EGFR, p-EGFR, E-cadherin, and N-cadherin protein expression 48 h after transfecting T24/GR cells with MYLK siRNA. C. Western blot assay to detect MYLK, EGFR, p-EGFR, E-cadherin, and N-cadherin protein expression in T24/GR cells transfected with MYLK overexpression plasmid, with or without erlotinib treatment. When comparing the two groups, $*P < 0.05$, $**P < 0.01$, $***P < 0.001$, and $****P < 0.0001$ indicate significance.

of E-Cadherin were partially reversed by MYLK overexpression. These results demonstrate that MYLK functions upstream of EGFR in the regulatory pathway, and that the MYLK-EGFR

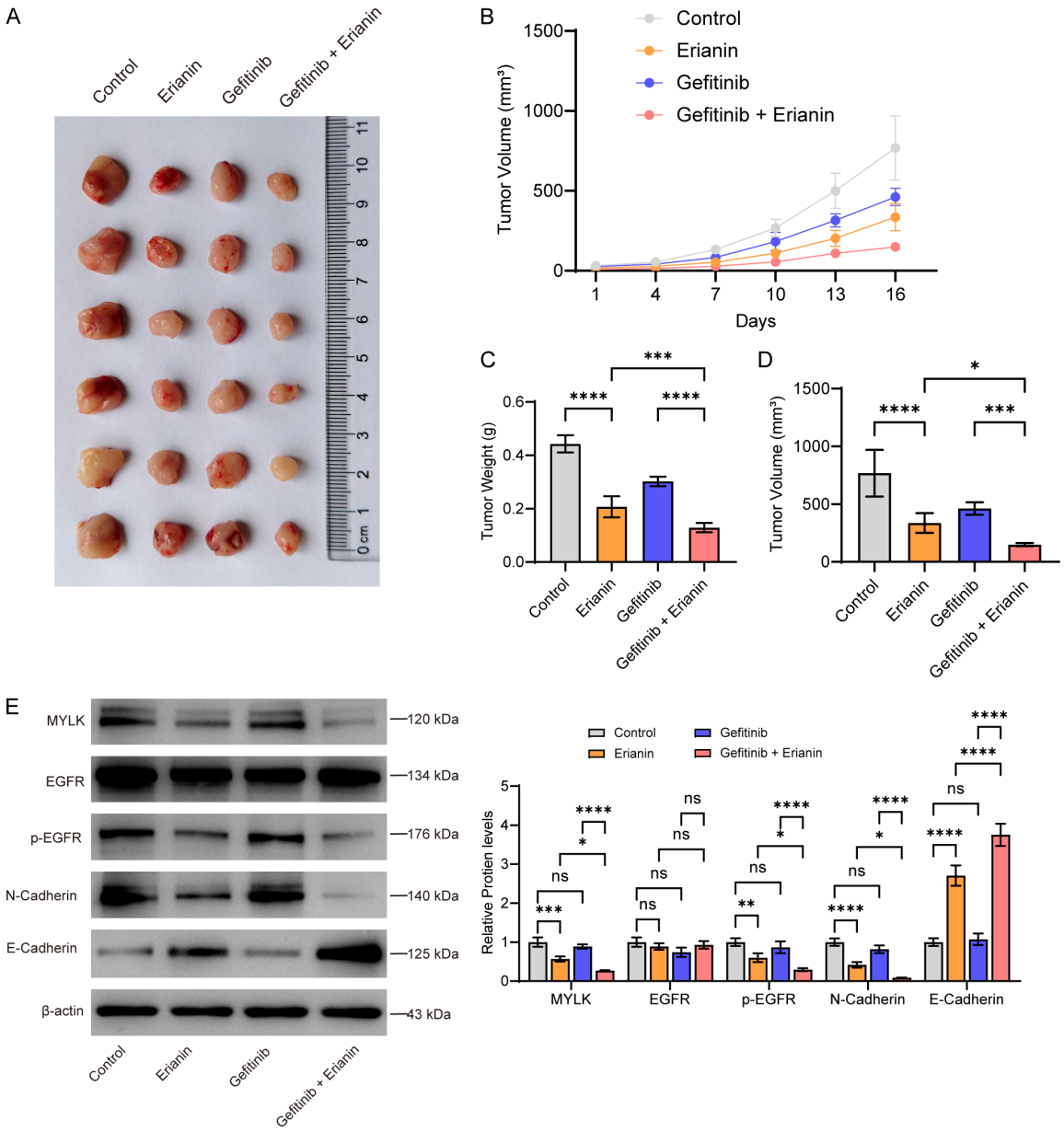


**Figure 7.** Erianin enhances gefitinib sensitivity in T24/GR xenograft mouse model. A. Representative images of dissected tumors from each group at the end of the experiment. B. Tumor growth curves showing changes in tumor volume over time in different treatment groups. C. Comparison of tumor weights among all groups at the endpoint. D. Comparison of final tumor volumes among all groups at the endpoint. E. Western blot analysis of MYLK, p-EGFR, EGFR, E-Cadherin, and N-Cadherin protein expression levels in tumor tissues from each group, with GAPDH or β-actin used as the loading control. When comparing the two groups, *$P < 0.05$, **$P < 0.01$, ***$P < 0.001$, and ****$P < 0.0001$ indicate significance.

axis plays a critical role in mediating EMT progression in T24/GR cells.

*Erianin enhances gefitinib sensitivity in T24/GR xenograft mouse model*

To further validate the therapeutic potential of erianin in restoring gefitinib sensitivity in vivo, a T24/GR xenograft nude mouse model was established. As shown in **Figure 7A**, tumors in the control group exhibited the largest volume, while combination treatment resulted in the smallest tumor size. Tumor growth curves demonstrated that both erianin and gefitinib monotherapy inhibited tumor growth to varying degrees; however, the combination of gefitinib

and erianin produced the most pronounced anti-tumor effect, with tumor volume being significantly smaller than that in the gefitinib alone group (**Figure 7B**). At the end of the experiment, tumor weight and final tumor volume measurements consistently showed that the combination group achieved the greatest therapeutic efficacy (**Figure 7C** and **7D**). Western blot analysis of tumor tissues revealed that erianin significantly downregulated MYLK, p-EGFR, and N-Cadherin expression, while upregulating E-Cadherin expression. Notably, gefitinib alone did not significantly affect MYLK expression, whereas the combination treatment resulted in the most substantial downregulation of MYLK and p-EGFR, accompanied by the strongest reversal of EMT markers (**Figure 7E**). These in vivo results further confirm that erianin restores gefitinib sensitivity by targeting the MYLK-EGFR axis, providing a promising therapeutic strategy for overcoming EGFR inhibitor resistance in bladder cancer.

## Discussion

Currently, no EGFR inhibitor has been officially approved for the clinical treatment of bladder cancer, and most EGFR-targeted drugs remain in clinical trials. Gefitinib, erlotinib, cetuximab, and dacomitinib have been extensively studied, although they are not approved for this indication [3-6]. Gefitinib was selected as the EGFR inhibitor in this study because EGFR is frequently highly expressed in bladder cancer and is associated with invasiveness and poor prognosis [35]. Gefitinib inhibits EGFR tyrosine kinase activity and blocks downstream EGFR-mediated signaling pathways, including ERK and Akt phosphorylation, thereby suppressing bladder cancer cell proliferation [36]. Several preclinical studies have demonstrated the potential value of gefitinib, including in combination with phenformin and glutamine blockers [10-12].

Erianin has anticancer activity in several cancers, although its role and mechanism in bladder cancer remain unclear [37, 38]. Gefitinib has specific activity as an EGFR-TKI in bladder cancer [39], whereas gefitinib resistance limits its anticancer effects [40]. We analyzed the intersection of target genes from three online databases and identified MYLK and AURKA as the final candidate genes. AURKA expression did not significantly affect prognosis in patients with bladder cancer, whereas patients with high MYLK expression had worse prognosis than those with low MYLK expression. MYLK is a pro-carcinogenic gene that induces cancer cell angiogenesis, invasion, and metastasis [41, 42], which may contribute to the poor prognosis of patients with high MYLK-expressing bladder cancer. In this study, MYLK was highly expressed in T24/GR cells, and erianin treatment inhibited their invasion and migration. MYLK overexpression attenuated the effects of erianin on T24/GR cells, whereas si-MYLK downregulation produced a stronger inhibitory effect on T24/GR cells. Subsequently, MYLK expression was positively correlated with of EGFR expression, and erianin reduced both EGFR and MYLK expression in T24/GR cells. MYLK4 activates EGFR in osteosarcoma to induce invasion and metastasis [43], whereas inhibition of MYLK expression can prevent invasion and metastasis in prostate [37] and breast cancers [38], consistent with the present findings. Erianin may affect EGFR expression by regulating MYLK, thereby restoring the sensitivity of bladder cancer cells to gefitinib. Co-immunoprecipitation further verified the interaction between MYLK and EGFR. MYLK4, a member of the MYLK family, is positively correlated with EGFR expression in osteosarcoma, and EGFR has been detected in the MYLK4 protein complex, suggesting an interaction between them [43]. This finding is consistent with the present results.

Bladder cancer invasion and migration are key factors associated with poor prognosis. EMT participates in malignant transformation and tumor cell migration, thereby promoting tumor progression and metastasis. E-cadherin expression is correlated with survival in patients treated with EGFR-TKIs [44], and both E- and N-cadherins are involved in gefitinib resistance [45]. In the present study, erianin inhibited EMT in T24/GR cells by regulating MYLK expression, resulting in increased E-cadherin expression and decreased N-cadherin expression. EMT inhibition reverses gefitinib resistance in lung adenocarcinoma [46], consistent with the present findings.

This study clarifies a mechanism by which erianin restores gefitinib sensitivity by targeting MYLK to regulate the EGFR/EMT pathway. This mechanism may be relevant to other EGFR-dependent tumor types with similar drug resis-

tance mechanisms, such as non-small cell lung cancer, and should be evaluated in relevant models.

Although these findings are promising, this study has some limitations. First, the relationship between MYLK and EGFR requires further investigation. EMT in cancer cells is a relatively complex process, and the present findings do not fully explain the specific mechanistic role of erianin in EMT. In addition, gefitinib resistance may involve multiple proliferation- and survival-related mechanisms, including the PI3K/AKT pathway [47, 48]. Because resistance mechanisms involving this pathway have been widely studied, this study focused on the EGFR and EMT pathways. Experimental evidence indicates that the EGFR-EMT axis has a central regulatory role in specific drug-resistance models. By identifying an MYLK-mediated regulatory mechanism, this study further clarifies the biological significance of this pathway. Finally, no combination index (CI) analysis was performed in this study. CI analysis would provide more rigorous quantification of the synergistic effect between erianin and gefitinib, and this should be addressed in future studies.

## Conclusion

This study screened potential erianin targets for bladder cancer treatment and confirmed that erianin regulates MYLK to inhibit EGFR expression, thereby restoring gefitinib sensitivity. These findings identify potential therapeutic strategies and target genes for gefitinib-resistant bladder cancer, providing a theoretical basis for further studies.

## Acknowledgements

We thank the Beijing Yaohe Biotechnology Co., China, for providing western blot technical support. This study was supported by Hebei Provincial Government Funded Clinical Medicine Excellent Talent Project (ZF2024233). The Excellent Going Abroad Experts' Training Program in Hebei Province (202028).

## Disclosure of conflict of interest

None.

**Address correspondence to:** Fan Xu, Department of Oncology, Affiliated Hospital of Chengde Medical University, No. 36, Nanyingzi Street, Shuangqiao District, Chengde 067000, Hebei, China. Tel: +86-0314-2270940; E-mail: xfhebcd@163.com

## References

[1] Cathomas R, Lorch A, Bruins HM, Compérat EM, Cowan NC, Efstathiou JA, Fietkau R, Gakis G, Hernández V, Espinós EL, Neuzillet Y, Ribal MJ, Rouanne M, Thalmann GN, van der Heijden AG, Veskimäe E, Alfred Witjes J and Milowsky MI; EAU Muscle-invasive, Metastatic Bladder Cancer Guidelines Panel. The 2021 updated European association of urology guidelines on metastatic urothelial carcinoma. Eur Urol 2022; 81: 95-103.

[2] Al-Husseini MJ, Kunbaz A, Saad AM, Santos JV, Salahia S, Iqbal M and Alahdab F. Trends in the incidence and mortality of transitional cell carcinoma of the bladder for the last four decades in the USA: a SEER-based analysis. BMC Cancer 2019; 19: 46.

[3] Chism DD. Urothelial carcinoma of the bladder and the rise of immunotherapy. J Natl Compr Canc Netw 2017; 15: 1277-1284.

[4] Lopez-Beltran A, Cookson MS, Guercio BJ and Cheng L. Advances in diagnosis and treatment of bladder cancer. BMJ 2024; 384: e076743.

[5] Loriot Y, Matsubara N, Park SH, Huddart RA, Burgess EF, Houede N, Banek S, Guadalupi V, Ku JH, Valderrama BP, Tran B, Triantos S, Kean Y, Akapame S, Deprince K, Mukhopadhyay S, Stone NL and Siefker-Radtke AO; THOR Cohort 1 Investigators. Erdafitinib or chemotherapy in advanced or metastatic urothelial carcinoma. N Engl J Med 2023; 389: 1961-1971.

[6] van der Heijden MS, Sonpavde G, Powles T, Necchi A, Burotto M, Schenker M, Sade JP, Bamias A, Beuzeboc P, Bedke J, Oldenburg J, Chatta G, Ürün Y, Ye D, He Z, Valderrama BP, Ku JH, Tomita Y, Filian J, Wang L, Purcea D, Patel MY, Nasroulah F and Galsky MD; CheckMate 901 Trial Investigators. Nivolumab plus gemcitabine-cisplatin in advanced urothelial carcinoma. N Engl J Med 2023; 389: 1778-1789.

[7] Meng X, Xiao W, Sun J, Li W, Yuan H, Yu T, Zhang X and Dong W. CircPTK2/PABPC1/SETDB1 axis promotes EMT-mediated tumor metastasis and gemcitabine resistance in bladder cancer. Cancer Lett 2023; 554: 216023.

[8] Wang R, Gao D, Chen C, Fan G, Cheng H, Tao Y, Lu J, Tian J, Wang Y and Wang Z. ADAM12 promotes gemcitabine resistance by activating EGFR signaling pathway and induces EMT in bladder cancer. Clin Transl Oncol 2023; 25: 1425-1435.

[9] Wu YS, Ho JY, Yu CP, Cho CJ, Wu CL, Huang CS, Gao HW and Yu DS. Ellagic acid resensitizes gemcitabine-resistant bladder cancer cells by

inhibiting epithelial-mesenchymal transition and gemcitabine transporters. Cancers (Basel) 2021; 13: 2032.
[10] Ma G, Jia H, Li Z, Zhang X, Wang L, Zhang Z, Xiao Y, Liang Z, Li D, Chen Y, Tian X, Wang Y, Liang Y and Niu H. Gefitinib reverses PD-L1-mediated immunosuppression induced by long-term glutamine blockade in bladder cancer. Cancer Immunol Res 2025; 13: 66-83.
[11] Huang Y, Zhou S, He C, Deng J, Tao T, Su Q, Darko KO, Peng M and Yang X. Phenformin alone or combined with gefitinib inhibits bladder cancer via AMPK and EGFR pathways. Cancer Commun (Lond) 2018; 38: 50.
[12] Peng M, Huang Y, Tao T, Peng CY, Su Q, Xu W, Darko KO, Tao X and Yang X. Metformin and gefitinib cooperate to inhibit bladder cancer growth via both AMPK and EGFR pathways joining at Akt and Erk. Sci Rep 2016; 6: 28611.
[13] Fan T, Li S, Xiao C, Tian H, Zheng Y, Liu Y, Li C and He J. CCL20 promotes lung adenocarcinoma progression by driving epithelial-mesenchymal transition. Int J Biol Sci 2022; 18: 4275-4288.
[14] Xie Y, Zhu S, Zang J, Wu G, Wen Y, Liang Y, Long Y, Guo W, Zang C, Hu X, Fan G, Xiang S and Zhang J. ADNP prompts the cisplatin-resistance of bladder cancer via TGF-β-mediated epithelial-mesenchymal transition (EMT) pathway. J Cancer 2021; 12: 5114-5124.
[15] Ma X, Mao G, Chang R, Wang F, Zhang X and Kong Z. Down-regulation of autophagy-associated protein increased acquired radio-resistance bladder cancer cells sensitivity to taxol. Int J Radiat Biol 2021; 97: 507-516.
[16] Jin Y, Huynh DTN, Kang KW, Myung CS and Heo KS. Inhibition of p90RSK activation sensitizes triple-negative breast cancer cells to cisplatin by inhibiting proliferation, migration and EMT. BMB Rep 2019; 52: 706-711.
[17] Yan L, Zhang Z, Liu Y, Ren S, Zhu Z, Wei L, Feng J, Duan T, Sun X, Xie T and Sui X. Anticancer activity of erianin: cancer-specific target prediction based on network pharmacology. Front Mol Biosci 2022; 9: 862932.
[18] Chen MF, Liou SS, Kao ST and Liu IM. Erianin protects against high glucose-induced oxidative injury in renal tubular epithelial cells. Food Chem Toxicol 2019; 126: 97-105.
[19] Dou B, Hu W, Song M, Lee RJ, Zhang X and Wang D. Anti-inflammation of Erianin in dextran sulphate sodium-induced ulcerative colitis mice model via collaborative regulation of TLR4 and STAT3. Chem Biol Interact 2020; 324: 109089.
[20] Liu Z, Huang L, Sun L, Nie H, Liang Y, Huang J, Wu F and Hu X. Ecust004 suppresses breast cancer cell growth, invasion, and migration via EMT regulation. Drug Des Devel Ther 2021; 15: 3451-3461.
[21] Yang L, Hu Y, Zhou G, Chen Q and Song Z. Erianin suppresses hepatocellular carcinoma cells through down-regulation of PI3K/AKT, p38 and ERK MAPK signaling pathways. Biosci Rep 2020; 40: BSR20193137.
[22] Shi X, Yu X, Wang J, Bian S, Li Q, Fu F, Zou X, Zhang L, Bast RC Jr, Lu Z, Guo L, Chen Y and Zhou J. SIK2 promotes ovarian cancer cell motility and metastasis by phosphorylating MYLK. Mol Oncol 2022; 16: 2558-2574.
[23] Lin J, He Y, Chen L, Chen X, Zang S and Lin W. MYLK promotes hepatocellular carcinoma progression through regulating cytoskeleton to enhance epithelial-mesenchymal transition. Clin Exp Med 2018; 18: 523-533.
[24] Johnson M, Garassino MC, Mok T and Mitsudomi T. Treatment strategies and outcomes for patients with EGFR-mutant non-small cell lung cancer resistant to EGFR tyrosine kinase inhibitors: focus on novel therapies. Lung Cancer 2022; 170: 41-51.
[25] Shang L, Wang Y, Li J, Zhou F, Xiao K, Liu Y, Zhang M, Wang S and Yang S. Mechanism of Sijunzi decoction in the treatment of colorectal cancer based on network pharmacology and experimental validation. J Ethnopharmacol 2023; 302: 115876.
[26] He Z, Hu Y, Zhang Y, Xie J, Niu Z, Yang G, Zhang J, Zhao Z, Wei S, Wu H and Hu W. Asiaticoside exerts neuroprotection through targeting NLRP3 inflammasome activation. Phytomedicine 2024; 127: 155494.
[27] Cheng M, Li M, Zhang Y, Gu X, Gao W, Zhang S and Liu J. Exploring the mechanism of PPCPs on human metabolic diseases based on network toxicology and molecular docking. Environ Int 2025; 196: 109324.
[28] Zheng Z, Hu H, Zeng L, Yang H, Yang T, Wang D, Zhang C, Deng Y, Zhang M, Guo D and Deng F. Analysis of the characteristic compounds of Citri Sarcodactylis Fructus from different geographical origins. Phytochem Anal 2022; 33: 72-82.
[29] Zhang C, Liu J, Lai M, Li J, Zhan J, Wen Q and Ma H. Circular RNA expression profiling of granulosa cells in women of reproductive age with polycystic ovary syndrome. Arch Gynecol Obstet 2019; 300: 431-440.
[30] Pinzi L and Rastelli G. Molecular docking: shifting paradigms in drug discovery. Int J Mol Sci 2019; 20: 4331.
[31] Dong D, Xu Z, Zhong W and Peng S. Parallelization of molecular docking: a review. Curr Top Med Chem 2018; 18: 1015-1028.
[32] Pelikan A, Herzel H, Kramer A and Ananthasubramaniam B. Venn diagram analysis overestimates the extent of circadian rhythm reprogramming. FEBS J 2022; 289: 6605-6621.
[33] Lica JJ, Wieczór M, Grabe GJ, Heldt M, Jancz M, Misiak M, Gucwa K, Brankiewicz W, Maciejew-

ska N, Stupak A, Bagiński M, Rolka K, Hellmann A and Składanowski A. Effective drug concentration and selectivity depends on fraction of primitive cells. Int J Mol Sci 2021; 22: 4931.
[34] Caldwell GW, Yan Z, Lang W and Masucci JA. The IC(50) concept revisited. Curr Top Med Chem 2012; 12: 1282-1290.
[35] Rose M, Maurer A, Wirtz J, Bleilevens A, Waldmann T, Wenz M, Eyll M, Geelvink M, Gereitzig M, Rüchel N, Denecke B, Eltze E, Herrmann E, Toma M, Horst D, Grimm T, Denzinger S, Ecke T, Vögeli TA, Knuechel R, Maurer J and Gaisa NT. EGFR activity addiction facilitates anti-ERBB based combination treatment of squamous bladder cancer. Oncogene 2020; 39: 6856-6870.
[36] Weickhardt AJ, Lau DK, Hodgson-Garms M, Lavis A, Jenkins LJ, Vukelic N, Ioannidis P, Luk IY and Mariadason JM. Dual targeting of FGFR3 and ERBB3 enhances the efficacy of FGFR inhibitors in FGFR3 fusion-driven bladder cancer. BMC Cancer 2022; 22: 478.
[37] Xiang Y, Chen X, Wang W, Zhai L, Sun X, Feng J, Duan T, Zhang M, Pan T, Yan L and Jin T. Natural product erianin inhibits bladder cancer cell growth by inducing ferroptosis via NRF2 inactivation. Front Pharmacol 2021; 12: 775506.
[38] Zhu Q, Sheng Y, Li W, Wang J, Ma Y, Du B and Tang Y. Erianin, a novel dibenzyl compound in Dendrobium extract, inhibits bladder cancer cell growth via the mitochondrial apoptosis and JNK pathways. Toxicol Appl Pharmacol 2019; 371: 41-54.
[39] Facchinetti F, Hollebecque A, Braye F, Vasseur D, Pradat Y, Bahleda R, Pobel C, Bigot L, Déas O, Florez Arango JD, Guaitoli G, Mizuta H, Combarel D, Tselikas L, Michiels S, Nikolaev SI, Scoazec JY, Ponce-Aix S, Besse B, Olaussen KA, Loriot Y and Friboulet L. Resistance to selective FGFR inhibitors in FGFR-driven urothelial cancer. Cancer Discov 2023; 13: 1998-2011.
[40] Wei W, Zhang S, Han H, Wang X, Zheng S, Wang Z, Yang C, Wang L, Ma J, Guo S, Wang J, Liu L, Choe J and Lin S. NAT10-mediated ac4C tRNA modification promotes EGFR mRNA translation and gefitinib resistance in cancer. Cell Rep 2023; 42: 112810.
[41] Kassouf W, Luongo T, Brown G, Adam L and Dinney CP. Schedule dependent efficacy of gefitinib and docetaxel for bladder cancer. J Urol 2006; 176: 787-792.
[42] Paul MR, Pan TC, Pant DK, Shih NN, Chen Y, Harvey KL, Solomon A, Lieberman D, Morrissette JJ, Soucier-Ernst D, Goodman NG, Stavropoulos SW, Maxwell KN, Clark C, Belka GK, Feldman M, DeMichele A and Chodosh LA. Genomic landscape of metastatic breast cancer identifies preferentially dysregulated pathways and targets. J Clin Invest 2020; 130: 4252-4265.
[43] Yang M, Zhang T, Zhang Y, Ma X, Han J, Zeng K, Jiang Y, Wang Z, Wang Z, Xu J, Hua Y, Cai Z and Sun W. MYLK4 promotes tumor progression through the activation of epidermal growth factor receptor signaling in osteosarcoma. J Exp Clin Cancer Res 2021; 40: 166.
[44] Xing RC, Zheng J, Zheng WH, Qin ZP, Liu W and Yao RC. Relevance of E-cadherin expression to EGFR-TKI molecular targeted therapy sensitivity/resistance and its clinical significance. Genet Mol Res 2015; 14: 5785-5792.
[45] Witta SE, Dziadziuszko R, Yoshida K, Hedman K, Varella-Garcia M, Bunn PA Jr and Hirsch FR. ErbB-3 expression is associated with E-cadherin and their coexpression restores response to gefitinib in non-small-cell lung cancer (NSCLC). Ann Oncol 2009; 20: 689-695.
[46] Wei J, Li Y, Xu B and Yu J. Astragalus polysaccharides reverse gefitinib resistance by inhibiting mesenchymal transformation in lung adenocarcinoma cells. Am J Transl Res 2020; 12: 1640-1657.
[47] Zhang J, Qu Z, Xiao X, Adelson DL, Wang F, Wei A, Harata-Lee Y, Cui J, He D, Xie L, Sun L, Li J, Huang Z, Aung T, Yao H and Lin L. A novel sensitizer reduces EGFR-TKI resistance by regulating the PI3K/Akt/mTOR pathway and autophagy. Heliyon 2025; 11: e41104.
[48] Song H, Liu D, Dong S, Zeng L, Wu Z, Zhao P, Zhang L, Chen ZS and Zou C. Epitranscriptomics and epiproteomics in cancer drug resistance: therapeutic implications. Signal Transduct Target Ther 2020; 5: 193.

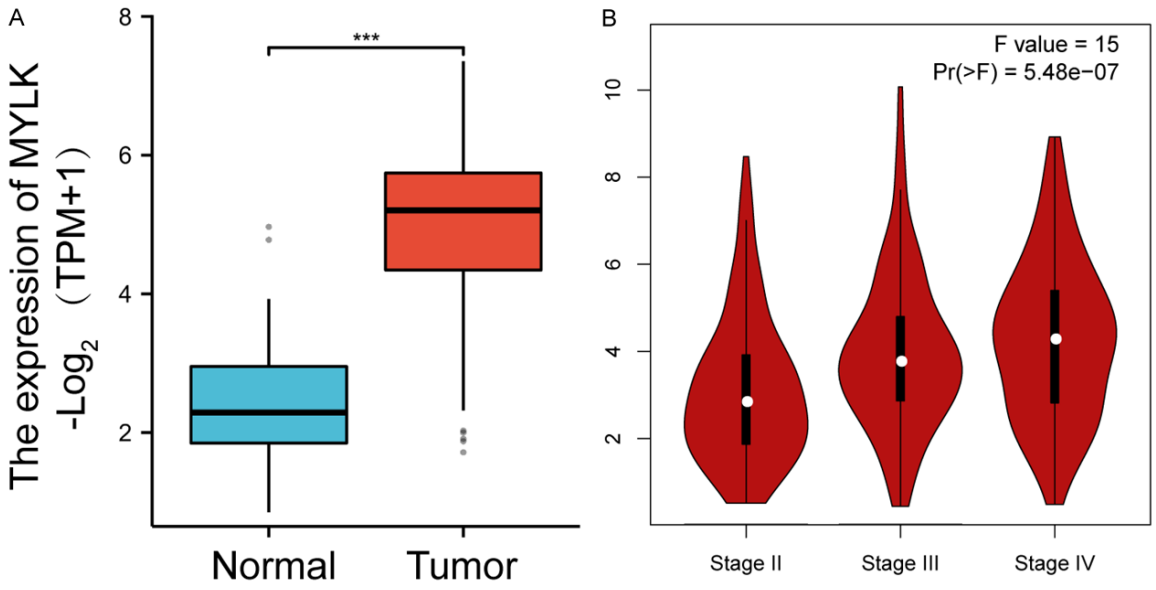


**Figure S1.** Analysis of the correlation between MYLK expression profiles and clinical staging. A. Box plot showing MYLK expression in normal (blue) and tumor (red) tissues. B. Violin plot illustrating the distribution density and expression trends of MYLK across different clinical stages (Stage II, III, and IV) of bladder cancer.

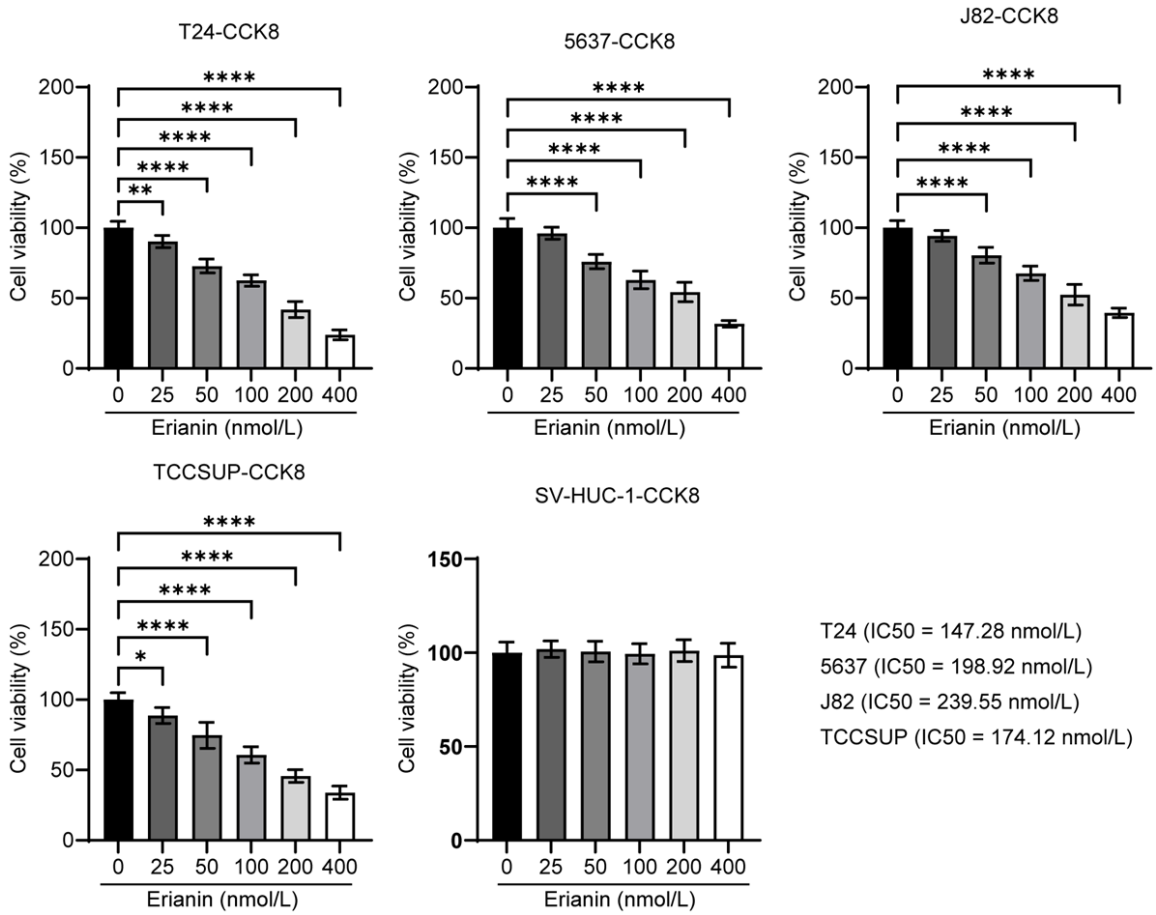


**Figure S2.** Erianin inhibits the proliferation of bladder cancer cells. The CCK8 assay was used to detect the changes in cell viability after treating T24, 5637, J82, TCCSUP, and SV-HUC-1 cells with different concentrations of Erianin (25, 50, 100, 200, 400 nmol/L) for 48 h. The IC50 of Erianin on bladder cancer cells was calculated using GraphPad Prism 9.5.0.

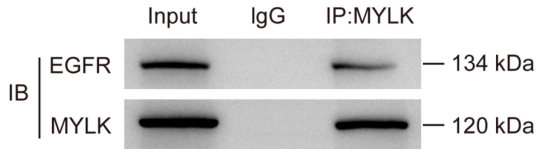


**Figure S3.** MYLK and EGFR can interact with each other. Detect whether there is an interaction between MYLK and EGFR in T24/GR cells through co-immunoprecipitation experiments.